**Modeling of Casting, Welding, and Advanced Solidification Processes - XII**
*Edited by: Steve L. Cockcroft and Daan M. Maijer*
***TMS (The Minerals, Metals & Materials Society), 2009***

# A PHASE FIELD MODEL FOR A GEOMETRICAL DESCRIPTION OF MICROPORES CONSTRAINED BY A SOLID NETWORK

M. Felberbaum, A. Jacot

Computational Materials Laboratory,
Ecole Polytechnique Fédérale de Lausanne, Station 12, Lausanne, Switzerland

Keywords: Porosity, Aluminum, Phase Field Modeling, Pore Pinching.

## Abstract

A 2D phase field model has been developed to describe the shape of a pore formed within interdendritic liquid channels. The influence of the solid, which can force the pore to adopt a non-spherical shape, is taken into account through the geometry of the domain and appropriate boundary conditions. The results show that the presence of solid can substantially influence the volume and pressure of the pore. A pore constrained to grow in narrow liquid channels exhibits a substantially higher mean curvature, a larger pressure and a smaller volume as compared with a pore grown under unconstrained conditions. The effect of pore pinching by the solid network was also evidenced by 3D characterization of a pore by X-ray tomography. These measurements showed high interface curvatures corresponding to an overpressure of more than 400 kPa.

## Introduction

Microporosity is one of the major defects encountered in solidification processes. The presence of micropores can considerably reduce the mechanical properties of a cast material, in particular the fatigue life and the ultimate tensile strength [1]. The basic mechanisms responsible for the formation of micropores are well established. Solidification shrinkage, i.e. the difference in specific volume between the liquid and solid phases, is known to play a key role. If shrinkage cannot be compensated by liquid flow in the mushy zone due to limited permeability, large pressure drops may develop and lead to the formation of pores. Gas dissolved in the liquid metal, such as hydrogen in aluminum alloys, can substantially contribute or even govern the formation of micropores. Due to a lower solubility in the solid phase, gas concentrate in the remaining liquid as solidification proceeds and may reach the critical concentration for the nucleation of a bubble. Once a pore has nucleated, it becomes a sink for the gas supersaturated in the liquid phase and it will grow until thermodynamic equilibrium is reached.
Modeling the formation of porosity in castings has been a subject of research for several decades. The reader is invited to refer to the review article of Lee *et al* [2]. State-of-the-art computer models describing the formation of microporosity on the scale of the casting process are based on volume-averaging methods for the calculation of the local temperature and pressure fields in the interdendritic liquid. These quantities are then used to estimate the level of gas segregation and to determine if conditions for the nucleation of a pore are met. After nucleation, the growth rate of the pores is calculated by solving a hydrogen mass balance. By coupling such an approach with a resolution of the micro-macro hydrogen transport in the melt, Carlson *et al* [3] incorporated the effects of finite-rate hydrogen diffusion into porosity modeling, an aspect that had been previously experimentally highlighted by Lee and co-workers [4]. Couturier *et al* [5], who used the same technique as Pequet *et al* [6] for the mesh refinement in the mushy zone, examined the influence of alloy components.

One aspect that has not previously been examined is the effect of pore morphology, and more specifically, the radius of curvature as it directly influences the gas pressure in the pore. As pores usually develop at high volume fractions of solid, they adopt complex shapes due to numerous contacts with neighboring dendrites arms. Very few studies have been devoted so far to this effect, although it is potentially important. The objective of the present work is to present a preliminary phase-field approach for a numerical description of the morphology of a pore constrained by a dendritic network. X-ray tomography experiments are first presented to show the importance of this phenomenon during solidification.

## Experimental

X-ray tomography experiments have been carried out in order to characterize the morphology of micropores in cast aluminum alloys. Al-4.5wt%Cu ingots (60 mm of diameter, 110 mm of height) were directionally solidified under controlled conditions (solidification rate of 1 mm/s, and thermal gradient of 30 K/cm). From these ingots, samples were extracted and analyzed by X-ray tomography using the TOMCAT beamline at the Swiss Light Source and a 0.7 μm camera pixel size.
From the 3D volume data, the mean curvature was then calculated for every pore larger than 50 $\mu m^3$, and at every point on the pore surface using the open source program *VTK* [7]. Figure 1 shows a volume rendering of one pore pinched by a dendritic network. As can be seen on the curvature distribution for this pore shown in Figure 2, the mean curvature can be larger than 0.2 $\mu m^{-1}$, which corresponds to a Laplace – Young overpressure of more than 400 kPa. As the pore must have a positive pressure, the mean value of the distribution is positive (black dot at 0.083 $\mu m^{-1}$ in Figure 2).

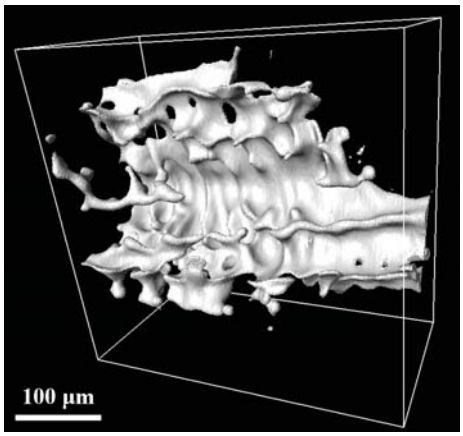


Figure 1: Volume rendering of a pore pinched in an Al-4.5wt%Cu matrix observed by X-ray tomography.

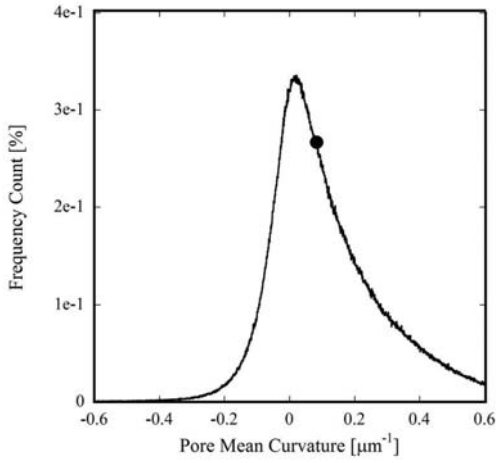


Figure 2: Mean curvature distribution of the pore illustrated in Figure 1. The dot represents the mean value of the distribution.

## Model

A phase field model has been developed in order to describe the shape of a pore forming within an interdendritic liquid channel and the geometrical effect of mechanical contacts with neighboring solid. The problem is solved in a domain that is representative of a small section of an interdendritic liquid channel. In this preliminary approach, only the evolution of the liquid/gas

interface is considered. The influence of the solid, which can force the pore to adopt a non-spherical shape, is taken into account through the geometry of the calculation domain and the boundary conditions, considering that the exterior of the domain corresponds to solidified regions.

The evolution of the liquid/gas interface is described with a phase equation using a similar approach as in solidification phase-field models [8]. The major difference lies in the driving force, which is given here by the pressure difference between the interior of the pore and the surrounding liquid.

In the current work, the following phase equation has been used:

$$\dot{\phi} = M\left[\varepsilon_\phi^2 \nabla^2 \phi - 2W\phi(1-\phi)(1-2\phi) - 30\phi^2(1-\phi)^2\left(p_p - p_l\right)\right] \qquad \text{Eq 1}$$

with

$$M = \frac{M_0}{6\delta}, \qquad \varepsilon^2 = 6\gamma_{lg}\delta \qquad \text{and} \qquad W = \frac{3\gamma_{lg}}{\delta}$$

where $\phi$ is the phase variable, which varies continuously through the interface from 0 in the liquid to 1 in the pore, $p_p$ is the pressure in the pore and $p_l$ is the pressure in the liquid. The parameters $M$, $W$, $\delta$ and $\gamma_{lg}$ correspond respectively to the interface mobility coefficient, the double-well height, the interface thickness and the liquid/gas interfacial energy.

By solving the steady-state form of Eq. 1 in cylindrical coordinates, one can show easily that the Laplace pressure condition, $p_p - p_l = 2\gamma_{lg} / r$ is recovered for a given pore radius, $r$, justifying in this way the form of this equation.

In this preliminary approach, the growth kinetics are assumed to be governed by hydrogen diffusion in the liquid, which, as pointed out by Lee and Carlson [3, 4], can be the limiting factor. (Hereafter the gas responsible for porosity will always be referred to as hydrogen, although the model could apply to other systems as well.) A local volumetric molar concentration of hydrogen is introduced based on an averaging procedure and considering $\phi$ as a local volume fraction of phase:

$$c^H = \phi c_l^H + (1-\phi)c_p^H \qquad \text{Eq 2}$$

where $c_l^H$ and $c_p^H$ are volumetric molar concentrations of hydrogen in the liquid and in the gas, respectively.

Assuming thermodynamic equilibrium at the interface, $c_l^H$ can be expressed as a function of $p_p$ using Sievert's law:

$$c_l^H = S_l\sqrt{\frac{p_p}{p_0}} \qquad \text{Eq 3}$$

where $S_l$ is the Sievert's constant (in atomic moles/m$^3$) and $p_0$ is the standard pressure. Introducing also the perfect gas law, Eq. 2 can be rewritten as:

$$c^H = \phi S_l\sqrt{\frac{p_p}{p_0}} + (1-\phi)\frac{2p_p}{RT} \qquad \text{Eq 4}$$

A hydrogen conservation equation is then solved, neglecting any hydrogen concentration gradient in the gas phase and any hydrogen transport in the liquid due to flow:

$$\frac{\partial c^H}{\partial t} = \nabla \cdot \left( \phi D_l^H \nabla c_l^H \right) \qquad \text{Eq 5}$$

The resolution of Eq. 1 and Eq. 5 is performed using a finite difference method and an explicit time-discretization scheme. At each time-step, the solution of Eq. 5 is used to calculate the driving force term of the phase equation. This requires solving the second order polynomial expression of Eq. 4 to obtain $p_p$ from $c^H$. An averaging procedure eliminating any concentration gradient in the pore is applied at every time-step.
The contact angle between the liquid/gas interface and the domain border (i.e. with the solid) is prescribed with a Dirichlet boundary conditions for the phase-field, using the approach developed by Sémoroz *et al* [9]. The average mean curvature of the pore is calculated using following expression:

$$\kappa = \frac{\int_\Omega \phi^2 \left(1-\phi\right)^2 \nabla \cdot \left( \frac{\nabla \phi}{|\nabla \phi|} \right) \mathrm{d}\Omega}{\int_\Omega \phi^2 \left(1-\phi\right)^2 \mathrm{d}\Omega}. \qquad \text{Eq 6}$$

since $\mathbf{n} = \nabla\phi / |\nabla\phi|$ is the normal to the interface and $\nabla \cdot \mathbf{n}$ represents the mean curvature of a sharp interface.

## Results and Discussion

A first test was carried out in order to test the capability of the model to correctly calculate the pressure and the radius of a spherical pore for a given set of conditions in terms of hydrogen content in the calculation domain, $c_0$, hydrogen solubility, $S_l$, and liquid pressure, $p_l$. The calculation was performed in a 2D square domain at the center of which a pore was initialized with an arbitrary radius. Once steady state is reached, the pore radius, $r$, and the pore pressure, $p_p$, can be compared with the analytical solution that is obtained from the following set of equations:

$$c_l^H = S_l \sqrt{\frac{p_p}{p_0}} \qquad \text{Eq 7}$$

$$p_p = \frac{c_p^H}{2} RT \qquad \text{Eq 8}$$

$$p_p - p_l = \frac{\gamma_{\mathrm{lg}}}{r_{eq}} \qquad \text{Eq 9}$$

$$\pi r_{eq}^2 c_p^H + \left( V_{comp} - \pi r_{eq}^2 \right) c_l^H = V_{comp} c_0 \qquad \text{Eq 10}$$

where $r_{eq}$ is the equilibrium radius of the circular pore and $V_{comp}$ is the volume of the calculation domain.
Table 1 summarizes the different parameters used in the calculation. The calculation was started with an initial pore size about 10 times smaller than $r_{eq}$. The initial gas content and pressure in the pore were chosen in order to satisfy the Laplace-Young equation and the perfect gas law. The hydrogen content in the domain was set to 25 mol/m$^3$, which is much larger than the equilibrium

concentration given by Sievert's law for the initial pore radius. As the liquid is supersaturated in hydrogen, the pore is expected to grow.

Table 1: parameters used in the phase-field calculations.

| Parameters | symbol, unit | numerical value |
|---|---|---|
| *Mesh size* | $a$ [m] | $2.5\times10^{-8}$ |
| *Volume of the calculation domain* | $V_{comp}$ [$m^3$] | $1.5625\times10^{-10}$ |
| *Contact angle of the l/g interface at the boundaries* | $\theta$ [-] | $\pi/3$ |
| *Interface thickness* | $\Delta$ [m] | $4\times10^{-8}$ |
| *Atmospheric pressure* | $p_0$ [Pa] | 101325 |
| *Liquid pressure* | $p_l$ [Pa]] | 101325 |
| *Temperature* | $T$ [K] | 1000 |
| *Interface mobility coefficient* | $M_0$ [$m^2$s/kg] | $1\times10^{-6}$ |
| *Hydrogen diffusion coefficient in liquid aluminum* | $D_l$ [$m^2$/s] | $1\times10^{-6}$ |
| *Sieverts' constant* | $S_l$ [mol/$m^3$] | 0.69 |
| *Liquid-gas interfacial energy* | $\gamma_{lg}$ [J/$m^2$] | 0.8 |

As can be seen in Figure 3, the pore radius calculated with the phase-field model increases rapidly, whereas its pressure decreases, until a steady-state is reached at a time of about $5\times10^{-5}$ s. Both the pressure and the radius of the pore stabilize very close to the analytical solution. Similar calculations started with different pore radii, either larger or smaller than $r_{eq}$, yielded the same steady state solution. Thus, the phase-field model is capable of correctly describing a bubble in equilibrium with its surrounding liquid, satisfying simultaneously the mechanical and chemical equilibrium conditions.

The transient regime of the calculation corresponds to the time required to homogenize the hydrogen concentration in the liquid. Although hydrogen diffusion can be the limiting factor for pore growth, the transient regime of the simulation cannot be exploited quantitatively in this preliminary approach. The reason is that the liquid flow induced by the expansion of the bubble, and thereby hydrogen transport by convection, are not considered in the simulation. For this reason only the steady state solutions of the simulation will be discussed hereafter.

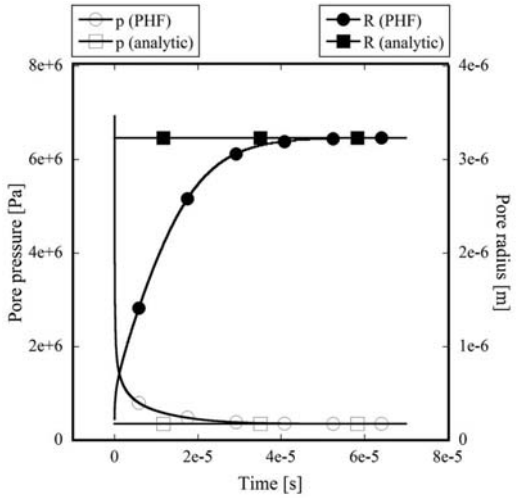


Figure 3: Radius and pressure of a circular 2D pore calculated with the phase-field model and with the analytical solution for a hydrogen solubility in the liquid of $S_l$ = 0.69 mol/$m^3$ and an overall hydrogen content, $c_0$, of 25 mol/$m^3$.

The model was then used to investigate the morphology and the pressure in a pore growing under the constraint of a surrounding solid. The calculations were performed in a 2D domain composed of a series of rectangular channels connected together by a central canal (see Figure 4). This geometry is aimed at simulating the growth of a pore in between presumably fixed dendrite arms. The contact angle between the liquid/gas interface and the border was set arbitrarily to $\pi/3$ for all boundaries. The overall hydrogen content in the calculation domain, $c_0$, was set to 25 mol/m$^3$.
The calculation was initialized with a pore size 10 times lower than $r_{eq}$ without any contact with the boundaries. The other calculation parameters are given in Table 1.
As the liquid is supersaturated in hydrogen, the pore grows until some equilibrium is reached. The final shape of the pore is shown in Figure 4 for three different channel widths, $L$, but identical volumes of calculation. The pressure in the pore, the mean radius of curvature and the volume of the pore were extracted from the calculations once a steady state was reached. The results are presented in Figure 5 and 6.

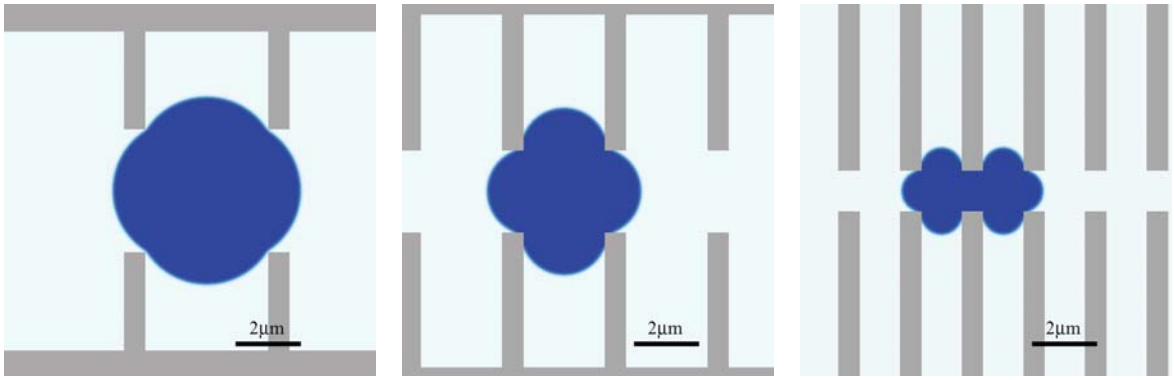


$L$ = 3.725 µm $L$ = 2.475 µm $L$ = 1.225 µm

Figure 4: Equilibrium pore shape for different liquid channel widths, $L$.

As can be seen in Figure 5, a smaller channel width leads to a higher pressure, a higher radius of curvature and a lower pore volume as compared with a less constrained pore. This effect is directly related to the fact that the growth of a pore inside a narrow liquid channel requires highly curved gas/liquid interfaces in order to satisfy the contact angles that have been prescribed on the boundary. The pressure in the pore is consequently larger in such pores since the Laplace - Young equation has to be satisfied.

The effect of the constraining solid can also be observed in Figure 6, which shows that the average mean radius of curvature becomes substantially smaller than the unconstrained radius when the channel width is small.
In the calculations shown here the influence of the solid morphology on the volume fraction and the morphology of the pores is substantial. By dividing the channel width by a factor 3 the pressure raises and the volume drops also by similar factor. The magnitude of this effect is naturally linked to the fact that the channel widths used in the calculations are rather small. However such narrow liquid channels are not unrealistic at the end of solidification.

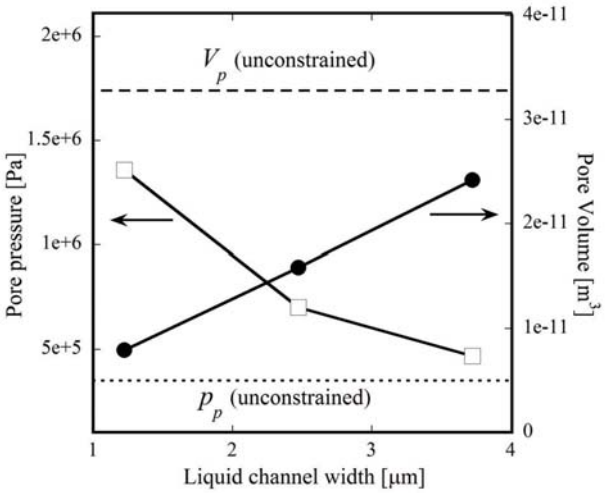


Figure 5: Effect of liquid channel width on pore pressure (squares) and pore volume (dots) calculated with the phase-field model. The dashed and dotted lines represent respectively the unconstrained pore volume and unconstrained pore pressure.

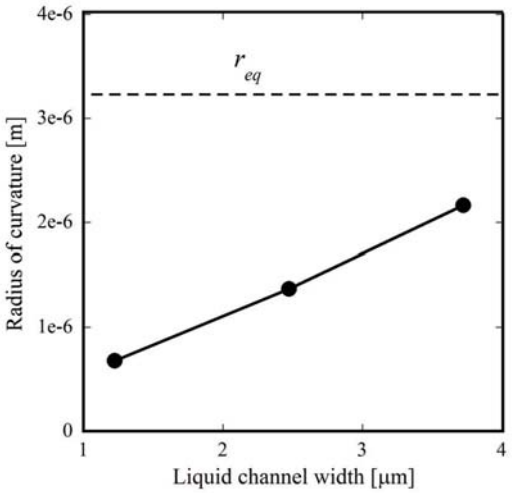


Figure 6: Effect of liquid channel width on the mean radius of curvature of a pore calculated with the phase-field model (see Eq. 6). The dashed line represents the unconstrained equilibrium radius of curvature.

The calculations presented here were performed with very high hydrogen contents (25 mol/m$^3$). These values become more realistic if one considers that the calculation domain is a small window centered on a pore, or in other words, that the simulation is focused on a particular area of the microstructure where the hydrogen content is locally very high. In this prospect, it is interesting to calculate, for a given pore volume and morphology obtained with the simulation, the number of pores per unit volume of liquid, $n_p$ , that should be considered in order to reach a given nominal hydrogen content per unit weight, $[H]_0$:

$$n_p = \frac{\rho[H]_0 - c_l^H}{V_p c_p^H} \qquad \text{Eq 11}$$

where $\rho$, $V_p$ and $c_l^H$ are the liquid density, the volume of the pore and the liquid concentration obtained in the simulation, respectively.
The calculation of $n_p$ yields directly the volume fraction of pores corresponding to a certain $[H]_0$:

$$g_p = \frac{1}{1 + V_p n_{pore}} \qquad \text{Eq 12}$$

The values of $g_p$ and $n_p$ corresponding to $[H]_0$ = 6.51 mol/m$^3$ (3 $cc_{STP}$/100g Al) have been reported in Table 2 for the unconstrained situation and for the 3 previously presented calculations at different channel widths. As can be seen, at fixed $[H]_0$, all calculations exhibit very similar conditions in terms of number of pores per unit volume. The major difference regarding the conditions of these calculations is thus essentially the size of the channel width. The large differences observed in the volume fractions of the pore and the pore pressure are therefore clearly due to the influence of the contacts with the solid, which may constrain the pore to adopt a high interface curvature and high pressure, if the liquid channels are narrow.

Table 2: Results of the simulations carried out with various liquid channel geometries.

| **Liquid channel width, $L$** | **Pressure in the pore, $p_p$** | **Pore volume, $V_p$** | **Radius of curvature $1/\kappa$** | **number of pore per unit volume, $n_p$ ($[H]_0 = cc_{STP}/100\ g_{Al}$)** | **volume fraction of pore, $g_p$ ($[H]_0 = 3cc_{STP}/100\ g_{Al}$)** |
|---|---|---|---|---|---|
| *[µm]* | *[Pa]* | *[$m^3$]* | *[m]* | *[$m^{-3}$]* | *[-]* |
| unconstrained | $3.48\times10^5$ | $3.29\times10^{-11}$ | $3.23\times10^{-6}$ | $1.90\times10^9$ | 5.88% |
| 3.725 | $4.68\times10^5$ | $2.42\times10^{-11}$ | $2.16\times10^{-6}$ | $1.85\times10^9$ | 4.28% |
| 2.475 | $7.02\times10^5$ | $1.58\times10^{-11}$ | $1.37\times10^{-6}$ | $1.76\times10^9$ | 2.71% |
| 1.225 | $13.6\times10^5$ | $7.91\times10^{-12}$ | $0.68\times10^{-6}$ | $1.54\times10^9$ | 1.21% |

## Conclusion

A 2D phase field model has been developed in order to describe the shape of a pore forming within interdendritic liquid channels and the geometrical effect of mechanical contacts with neighboring solid. The influence of the solid, which can force the pore to adopt a non-spherical shape, is taken into account through the geometry of the domain and appropriate boundary conditions. The results show that the presence of solid can substantially influence the volume and pressure of the pore. A pore constrained to grow in narrow liquid channels exhibits a higher mean curvature, a larger pressure and a smaller volume as compared with a pore grown under unconstrained conditions. The effect of pore pinching by the solid network was also evidenced by 3D characterization of a pore by X-ray tomography. It was shown that high values of the mean curvature can be reached locally, which corresponds to a Laplace – Young overpressure of more than 400 kPa.

Although the model accounts for hydrogen diffusion in the liquid, which is one of the main aspects governing the growth kinetics of a pore, this approach does not allow at this stage to correctly describe the dynamics of pore formation. To do so, the model should be combined with a description of the liquid flow induced by the pore growth. This would permit to properly take into account the effect of hydrogen transport by convection. In order to make a more quantitative investigation of the influence of the solid on the pore morphology the approach should be extended to 3D and an additional phase equation should be introduced to account for the evolution of the solid/liquid interface.

## References


1. Campbell, J., *Castings.* 2003
2. Lee, P.D., A. Chirazi, and D. See, *Journal of Light Metals*, 2001, **1**(1) p. 15-30
3. Carlson, K.D., Z. Lin, and C. Beckermann, *Metall. Mater. Trans. B*, 2007, **38**(4) p. 541-555
4. Lee, P.D. and J.D. Hunt, *Acta Materialia*, 1997, **45**(10) p. 4155-4169
5. Couturier, G. and M. Rappaz, *Modelling and Simulation in Materials Science and Engineering*, 2006, **14**(2) p. 253-271
6. Pequet, C., M. Gremaud, and M. Rappaz, *Metall. Mater. Trans. A*, 2002, **33**(7) p. 2095-2106
7. *The Visualization Tool Kit,* http://www.vtk.org/
8. Boettinger, W.J. *et al*, *Annu. Rev. Mater. Res*., 2001, **132** p. 163
9. Semoroz, A., S. Henry, and M. Rappaz, *Metall. Mater. Trans. A*, 2000, **31**(2) p. 487-495